Eur. Phys. J. A (2013) **49**: 69
DOI 10.1140/epja/i2013-13069-8

THE EUROPEAN PHYSICAL JOURNAL A

Special Article – Tools for Experiment and Theory

RPID — A new digital particle identification algorithm for CsI(Tl) scintillators

M. Bendel[1,a], R. Gernhäuser[1], W.F. Henning[1], R. Krücken[2,1], T. Le Bleis[1], and M. Winkel[1]

[1] Technische Universität München, Physik-Department E12, James-Franck-Str. 1, D-85748 Garching, Germany
[2] TRIUMF, 4004 Wesbrook Mall, Vancouver, BC, V6T 2A3, Canada

Received: 19 February 2013 / Revised: 8 May 2013
Published online: 11 June 2013 –
Communicated by J. Äystö

Abstract. A new digital algorithm for online particle identification in CsI(Tl), called *Reconstructive Particle IDentification* (RPID) is reported. The concept is based on a model for the signal generation with two exponential components for the scintillation light output and an exponential response function of the preamplifier. To provide a fast algorithm which could be used online in modern FPGA-based electronics a simplified method for signal deconvolution was developed. Within a few simple processing steps the original pulse shape is modified to recover the amplitudes of the two scintillation components that determine the type of particle. Data from an experiment $^{12}\mathrm{C}(\mathrm{p},\mathrm{p}')^{12}\mathrm{C}^*$ at 21 MeV allowed to separate γ-rays and protons even of very low energies. We present the performance of this new algorithm concerning the γ-proton separation as well as the identification of protons not fully stopped within the CsI(Tl).

1 Introduction

It is known for decades that the light output of thallium-doped cesium iodine (CsI(Tl)) crystals can be used for particle identification [1]. The scintillation process in this scintillator material is mainly based on two different scintillating states with significantly different lifetimes of about $\tau_\mathrm{f} = 0.6\,\mu$s and $\tau_\mathrm{s} = 3.25\,\mu$s [2]. Models of possible processes that lead to these decays are well described in the literature [3–8]. Already in 1958, Storey *et al.* [1] found out that the ratio of light output from the two main components depend on the ionization density of the absorbed particle [9,10] and therefore on the type of particle. A very good separation of γ-rays and particles with CsI(Tl) was reported already by Skulski *et al.* comparing different heuristic methods [11].

In this article we first discuss a model for the signal output of a charge-sensitive preamplifier connected to a Large Area Avalanche Photo Diode (LAAPD) that detects the scintillation light produced in a large volume CsI(Tl) scintillator and we show a new digital algorithm, the *Reconstructive Particle IDentification* (RPID) that allows to identify particles using the individual pulse shapes from the preamplifier directly recorded by standard flash ADCs. The underlying idea is to use different processing steps that modify the pulse shape in a way that allows to determine the amplitudes of the two main components directly. Additionally the RPID algorithm allows the implementation as firmware, *e.g.*, in a Field Programmable Gate Array (FPGA) for real-time particle identification. At present for many detector systems there is a transition to fully digital readout electronics. They are more flexible and in most cases also cheaper than common analog systems. Also the 4π calorimeter CALIFA [12], that will be built for the R^{3}B [13] experimental setup at FAIR and in which context this work was done, will be equipped with such a readout system.

2 Detector signal

Luminescent states of CsI(Tl) are assumed to be populated and depopulated by independent processes, following linear differential equations [14]. In a simplified model we first assume an excitation time constant much shorter than all the time constants important for depopulation [2]. If, like in CsI(Tl), only two main states contribute significantly to the scintillation light output, the time-dependent scintillation intensity $L(t)$ can be approximated by

$$L(t) = \frac{N_\mathrm{f}}{\tau_\mathrm{f}} e^{-\frac{t}{\tau_\mathrm{f}}} + \frac{N_\mathrm{s}}{\tau_\mathrm{s}} e^{-\frac{t}{\tau_\mathrm{s}}}, \qquad (1)$$

where $N_{\mathrm{f,s}} > 0$ are the integrated luminescences and $\tau_{\mathrm{f,s}}$ the characteristic decay time constants of the fast (f), respectively, the slow (s) component.

[a] e-mail: Michael.Bendel@tum.de

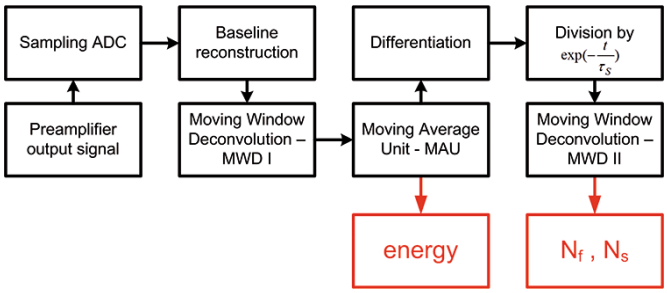

Fig. 1. schematic description of the RPID: the energy is determined after the first deconvolution, the RPID evaluation after the second. Further explanations are given in the text.

The scintillation light is converted to an electric pulse by a photomultiplier or by its semiconductor counterparts like Photo Diodes (PD), Silicon Photomultiplier (SiPM) or Avalanche Photo Diodes (APD). Within the subsequent charge-sensitive preamplifier the photo current is convolved with its response function G. In our case G is an exponential function with a decay time constant τ_p. The resulting voltage of an ideal charge-sensitive preamplifier output is

$$U(t) = \int_0^t L(t')G(t-t')\mathrm{d}t' = \int_0^t \left[\frac{N_\mathrm{f}}{\tau_\mathrm{f}} e^{-\frac{t'}{\tau_\mathrm{f}}} + \frac{N_\mathrm{s}}{\tau_\mathrm{s}} e^{-\frac{t'}{\tau_\mathrm{s}}}\right] e^{-\frac{t-t'}{\tau_p}} \mathrm{d}t'. \quad (2)$$

Usually $\tau_\mathrm{p} \gg \tau_{\mathrm{f,s}}$ is chosen to get a maximum fraction of signal and to minimize the ballistic deficit. Therefore energy measurements can be done after a Moving Window Deconvolution (MWD) [15,16] (see sect. 3.4).

3 Reconstructive Particle Identification – RPID

The information on the particle-species is contained in the dependence of the scintillation light on ionization density which is reflected by the ratio of N_f to N_s of eq. (2) [1]. In firmware, several processing steps are necessary to extract this information independently. These steps are summarized in fig. 1 and presented in more detail in the following sections.

The best separation for γ-rays and particles with CsI(Tl) was found by Skulski *et al.*, who compared different algorithms for their separation capabilities [11].

After the preamplifier signal is digitized in a sampling ADC, it is converted from a continuous analog function $U(t)$ to a digital time-discrete function $U(i \cdot t_\mathrm{s})$, where the time is segmented in multiples of the sampling interval t_s. If the time scale is normalized to t_s, eq. (2) becomes

$$U(i) = \sum_{i'=0}^{i} \left[\frac{N_\mathrm{f}}{m_\mathrm{f}} e^{-\frac{i'}{m_\mathrm{f}}} + \frac{N_\mathrm{s}}{m_\mathrm{s}} e^{-\frac{i'}{m_\mathrm{s}}}\right] e^{-\frac{i-i'}{m_\mathrm{p}}} \quad (3)$$

where $m_\mathrm{x} = \frac{\tau_\mathrm{x}}{t_\mathrm{s}}$.

3.1 Trigger

In this fully digital system also the triggers are generated digitally. A subtraction of two short integration windows delivers the slope in the beginning of an event signal and produces the trigger when exceeding a given threshold.

3.2 Baseline reconstruction

In a first step of the signal processing the baseline of the signal trace is reconstructed to eliminate baseline offsets as well as low frequency noise. Therefore the recorded samples are averaged and subtracted continuously from the trace. After an event is triggered, this algorithm is disabled and the current value is frozen for a certain time window, typically several preamplifier decay time constants, not to be altered by the signal. This method of course is rate-dependent and not feasible for too high rates, when the traces are dominated by pile-up events.

3.3 MWD I – Moving Window Deconvolution

Subsequent to the baseline reconstruction the exponential decay introduced by the preamplifier has to be eliminated.

Therefore a commonly used Moving Windows Deconvolution (MWD) algorithm [15] is used.

This processing method reconstructs the original charge function within the window L_1 produced by the scintillation light from the preamplifier output signal,

$$Q(i) = U(i) - U(i-L_1) + \frac{1}{m_\mathrm{p}} \sum_{i'=i-L_1}^{i} U(i'), \qquad i > 0, \quad (4)$$

where $i = 0$ is the trigger point, L_1 the MWD window size, m_p the decay time constant of the preamplifier (in units of t_s).

Applying this algorithm to the preamplifier output signal $U(i)$ described in eq. (3) results in the total charge function $Q(i)$, which is the integrated scintillation intensity function $L(i)$,

$$Q(i) = -N_\mathrm{f}\, e^{\left(-\frac{i}{m_\mathrm{f}}\right)} - N_\mathrm{s}\, e^{\left(-\frac{i}{m_\mathrm{s}}\right)} + N_\mathrm{f} + N_\mathrm{s}, \quad (5)$$

with the constraint of $N = N_\mathrm{f} + N_\mathrm{s}$ as the total charge produced by the scintillation light.

Applying a common Moving Average Unit (MAU) [17] with window size M to the deconvolved signal reduces the high frequency noise. It is worth noting that one can apply MWD or MAU in either order without changing the result [18].

3.4 Energy determination

A side effect of the MWD is the reconstruction of ballistic deficits. Especially for detectors with slow signal rise times, such as CsI(Tl) scintillators, it improves the energy resolution. Therefore the energy determination is placed after MWD I and MAU (see fig. 1) to take advantage of

this. Several methods exist to determine the energy. Peak sensing within the MWD window is a common method, but proportional to the remaining noise it generates a small average bias. This is avoided by a simple average over a few samples at a predetermined time after the trigger point. To gather most of the produced signal charge these samples are taken close to the end of the MWD window [19].

3.5 Differentiation

In the next step the total charge function $Q(i)$ is differentiated to recover the time-discrete detector current proportional to $L(i)$. The implementation is done as a subtraction of two sums within two short windows at constant distance $L_2 - N_1$.

The resulting function is the time discrete equivalent to eq. (1),

$$L(i) = \frac{N_\mathrm{f}}{m_\mathrm{f}} e^{-\frac{i}{m_\mathrm{f}}} + \frac{N_\mathrm{s}}{m_\mathrm{s}} e^{-\frac{i}{m_\mathrm{s}}}. \tag{6}$$

3.6 Division by an exponential function

An independent determination of N_f and N_s can be realized by dividing the scintillation function $L(i)$ by one of the two exponential functions (*e.g.*, the slow one with decay time constant m_s) of the scintillation signal. This results in a single exponential function with one time decay constant m_{sf} and a constant offset,

$$D(i) = \frac{N_\mathrm{f}}{m_\mathrm{f}} e^{-\frac{i}{m_\mathrm{sf}}} + \frac{N_\mathrm{s}}{m_\mathrm{s}} \tag{7}$$

with

$$m_\mathrm{sf} = \frac{m_\mathrm{s}\, m_\mathrm{f}}{m_\mathrm{s} - m_\mathrm{f}}. \tag{8}$$

In firmware this division can be obtained by multiplication with an exponential function with a positive exponent. This function is a property of the scintillator which does not change and its values can be calculated once and stored in a lookup table for faster online use in an FPGA.

3.7 MWD II

To eliminate the remaining exponential function, the moving window deconvolution is used for a second time with the decay time constant m_sf and window size L_2, with $L_2 < L_1$.

– Linear slope $0 < t < L_2$:

$$\begin{aligned} F(i) &= \frac{N_\mathrm{s}}{m_\mathrm{s}} \left(\frac{i}{m_\mathrm{sf}} + 1 \right) + \frac{N_\mathrm{f}}{m_\mathrm{f}} \\ &= m\, i + b. \end{aligned} \tag{9}$$

– Constant offset $L_2 < t < L_1$:

$$F(i) = \frac{N_\mathrm{s}}{m_\mathrm{s}} \frac{L_2}{m_\mathrm{sf}}. \tag{10}$$

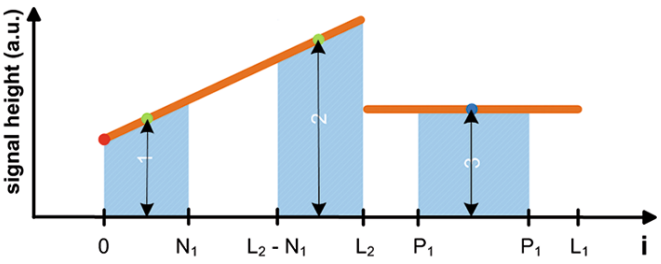

Fig. 2. After the RPID pulse shape analysis the signal has a linear slope in the beginning that is proportional to N_s with an offset that is proportional to $\frac{N_\mathrm{f}}{m_\mathrm{f}} + \frac{N_\mathrm{s}}{m_\mathrm{s}}$ and a constant offset in the end that is only proportional to N_s.

Due to the offset the integration generates a constant slope within L_2 (see fig. 2). The slope is directly proportional to the slow component N_s and the offset at the trigger time to $\frac{N_\mathrm{f}}{m_\mathrm{f}} + \frac{N_\mathrm{s}}{m_\mathrm{s}}$. Additionally, there is a constant baseline offset between L_2 and L_1 that is proportional to N_s. In the end there is only a small part of the trace that is used for the particle identification (see fig. 3). The beginning of the signal is smeared out by the MAU that is necessary to reduce noise and the end of the signal is dominated by the exponential decay of the preamplifier and contains less new information.

3.8 Evaluation and parameter setting

To extract the information, the linear slope m and its offset b can be determined by a simple linear regression algorithm.

$$m = \frac{\overline{xy} - \bar{x}\bar{y}}{\overline{x^2} - \bar{x}^2}, \tag{11}$$

$$b = \bar{y} - m\bar{x}. \tag{12}$$

For the use in FPGA-based real-time systems, the integration within two windows (fig. 2, window 1 + 2) with window size N_1 and a subsequent subtraction of the results is preferred due to the better performance. If for the first MWD window $L_1 \ll \tau_\mathrm{p}$, we can assume a slope m with L_2 points and a statistical normal distributed uncertainty Δy. The normalized uncertainty $\Delta m(N_1)$ then results in a function (13) with flat minimum at $N_1 = \frac{1}{3} L_2$,

$$\Delta m(N_1) = \sigma \frac{\sqrt{\frac{2}{N_1}}}{L_2 - N_1}, \tag{13}$$

where σ is the standard deviation of the normal distributed y values.

The estimation of the constant baseline offset at the end of the signal is also done by integrating within a certain window (fig. 2, window 3) to reduce noise contributions. The amplitudes N_f and N_s are then calculated by means of eqs. (9) and (10).

Several parameters of the RPID algorithm can be adjusted stepwise (see table 1, see sect. 4.2 below). The window size L_1 that is used for MWD I should be chosen

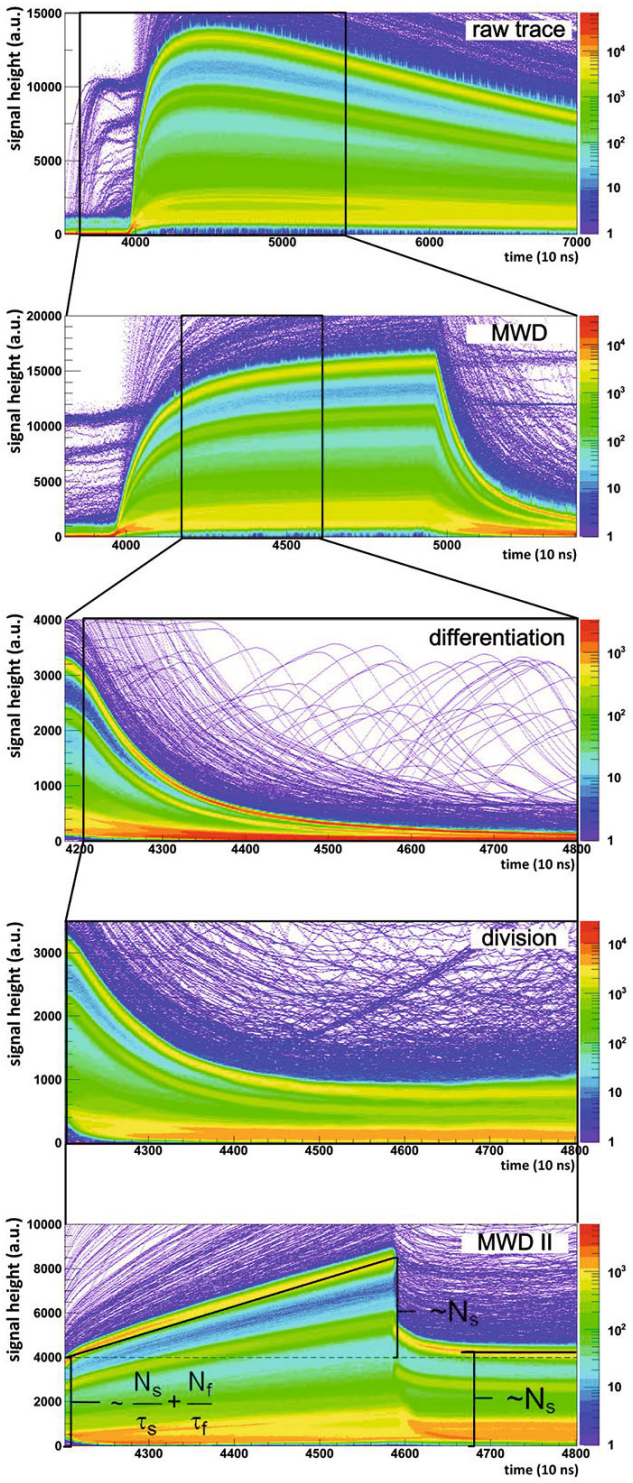

Fig. 3. Summary of digitized pulse shapes modified by the different major steps of the RPID algorithm. The data are taken from the experiment described in sect. 4. The picture represents an overlay about $2 \cdot 10^5$ different events covering the full range of accumulated shapes shown in fig. 5 and also pile-up. Further explanations are given in the text.

as large as needed to collect nearly the total amount of charge without introducing too much deadtime or losing an adequate pile-up rejection.

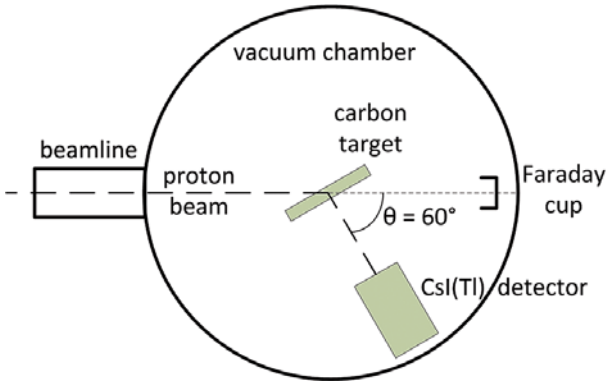

Fig. 4. Schematic drawing of the detector setup at the MLL.

For the division by one exponential, the time decay constant m_{sf} can be adjusted iteratively to result in one single exponential decaying function with a constant offset at the end, as stated in eq. (7). The parameters for MWD II are restricted by the additional constraint, that the decay time constant should be equal to m_{sf} (see eq. (8)). Again the constant offset in the transformed signal between L_2 and L_1 (see eq. (10) and fig. 2) is a good indicator for the accuracy of the used set of parameters.

4 Experiment

An experimental test of this new particle identification method was performed at the Munich Tandem accelerator (Maier-Leibnitz Laboratory (MLL), Garching), using a $^{12}\mathrm{C}(p,p')^{12}\mathrm{C}$ reaction [20] with a proton energy of $E_{\mathrm{kin}} = 21\,\mathrm{MeV}$. This allowed to obtain high energy scattered protons as well as γ-rays from inelastic scattering with energies up to 15.1 MeV [21] at the same time.

4.1 Experimental setup

The detector system consisted of three 130 mm long CsI(Tl) crystals with an entrance window of 15 mm × 25 mm. Each of them was read out by a Hamamatsu S8664-1010 Large Area Avalanche Photo Diode (LAAPD) [22–24] at a bias voltage of 420 V. For preamplification we used a Mesytec[1] MPRB-16 charge-sensitive preamplifier that was optimized to the high capacities of LAAPDs. Due to the strong temperature dependence of the internal APD gain [25] the preamplifier is operated with a temperature-dependent linear gain stabilization and a stabilization parameter of $\frac{\Delta V}{\Delta T} = 1.06\,\frac{\mathrm{V}}{^\circ\mathrm{C}}$ [26].

The detector was placed at an angle of $\theta = 60^\circ$ (fig. 4) with respect to the beam axis after a $75\,\mathrm{mg/cm^2}$ carbon target. Using a 16 bit sampling ADC (SIS 3302[2]) digital signal shapes with a length of 200 μs and a sampling frequency of 100 MHz were recorded.

[1] Mesytec – `http://www.mesytec.com`.

[2] Struck innovative systems – `http://www.struck.de/sis3302.htm`.

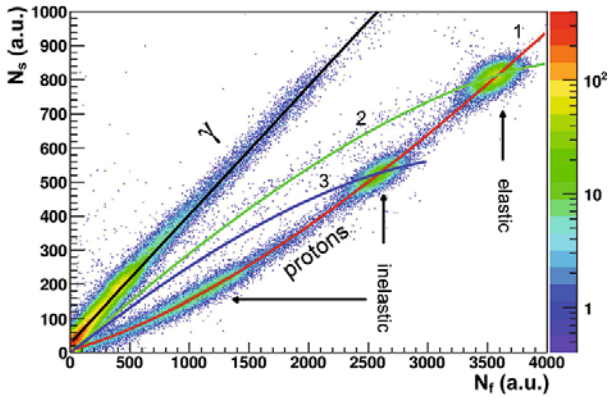

Fig. 5. First result of the *Reconstructive Particle Identification Algorithm (RPID)*. Photons and protons are well separated also for low energies. The red line (1) is fitted to the proton line and based on this fit, the green (2) and blue (3) lines are calculated as a function of scattered protons of two different energies that have not been stopped completely in one crystal.

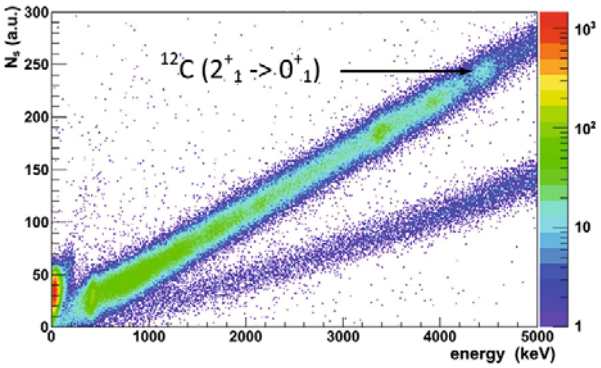

Fig. 6. For low energies the algorithm is still able to separate the photon and proton distribution. For better visualization of the range, N_f on the x-axis is replaced by the energy.

4.2 RPID parameters

The used RPID parameters for the ^{12}C experiment are summarized in table 1.

Table 1. Summary of the used RPID parameters in units of 10 ns.

MWD I	$L_1 = 1000$ $m_\mathrm{p} = 3965$
MAU	$M = 100$
Division	$m_\mathrm{s} = 325$
MWD II	$L_2 = 400$ $m_\mathrm{sf} = 75$

4.3 Experimental results

The pulse-shaped signals after applying the RPID algorithms are shown in fig. 3. The predicted shapes with a linear slope in the beginning and a constant offset in the end fit well to the obtained pulse shapes.

Figure 5 shows as a result of the RPID the reconstructed slow component of light emission *vs.* the respective fast component for the full unbiased set of experimental data.

Here the upper, rather straight distribution represents the γ-rays and due to a constant N_s-to-N_f ratio, a linear function (fig. 5, black line) fits well. The bent distribution below are protons.

Protons and γ-rays are separated accurately also for low energies (see fig. 6). The signal width for elastically and inelastically scattered protons is dominated by the target thickness, multiple scattering inside the target and inhomogeneous crystal wrapping. With our approach of reconstructing the real physical components of the scintillation light and using 130 mm long crystals as foreseen in calorimeters like CALIFA with rather small APD photo sensors, we achieved a clear separation in the full range from 16 MeV down to a fraction of 1 MeV. This separation is very similar to the best results reported by Skulski *et al.* [11] for low-energy protons and gammas indicating a limitation by the material itself. For low-energy protons there is a non-linear dependency between the two components. An empirical function $N_\mathrm{s}(N_\mathrm{f})$ (see eq. (14)) that is exponential for low energies and linear in the high energy range fits the proton distribution nicely (fig. 5, red line),

$$N_\mathrm{s,p}(N_\mathrm{f}) = a\left(e^{-bN_\mathrm{f}} - 1\right) + cN_\mathrm{f}. \tag{14}$$

From the data one can see that N_f is proportional to the energy and thus the derivative $\frac{\mathrm{d}N_\mathrm{s}}{\mathrm{d}E}$, respectively, $\frac{\mathrm{d}N_\mathrm{s}}{\mathrm{d}N_\mathrm{f}}$ specifies the $\frac{N_\mathrm{s}}{N_\mathrm{f}}$ dependency on the energy.

To calculate the N_s value for a particle that is completely stopped within the crystal, one integrates this derivative from 0 to $N_\mathrm{f,max}$, which corresponds to the energy of the incident proton. Of course this results in an $N_\mathrm{s,p}(N_\mathrm{f})$ function that is described in eq. (14).

If we assume now, that there are also protons that are scattered out of the crystal and leave it with a certain energy, the calculation has to be modified. In this case, one has to integrate from $N_\mathrm{f,min}$ which corresponds to the energy of the proton, when leaving the crystal to $N_\mathrm{f,max}$. That means $N_\mathrm{f,max} - N_\mathrm{f,min}$ corresponds to the energy deposited in the crystal and due to the assumed proportionality it equates to N_f. Carrying out the calculation with the integration limits $N_\mathrm{f,max}$ and $N_\mathrm{f,min} = N_\mathrm{f,max} - N_\mathrm{f}$ leads to

$$N_\mathrm{s,p,frac}(N_\mathrm{f}) = ae^{-bN_\mathrm{f,max}}\left(1 - e^{bN_\mathrm{f}}\right) + cN_\mathrm{f}. \tag{15}$$

In fig. 5, $N_\mathrm{s,p,frac}(N_\mathrm{f})$ is plotted for two different proton energies (blue and green line). Especially for the elastically scattered protons (green) that have high abundance, there is good agreement with the measured data. So by means of the RPID algorithm it is possible to distinguish between particles that have not been stopped and particles that have been fully stopped within one crystal. The

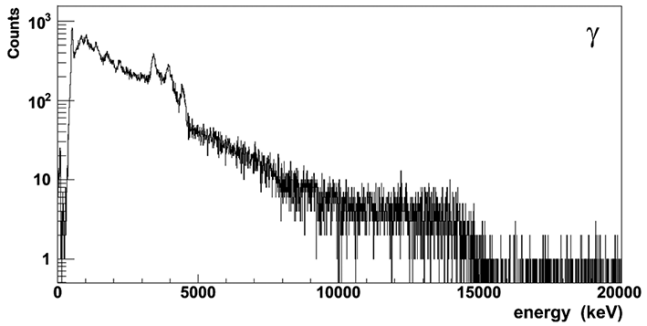

Fig. 7. γ-ray spectrum: By means of the RPID algorithm the proton and γ-ray spectra can be separated. The 4.4 MeV photopeak, single and double escape peak of the first 2^+ state in ^{12}C can be identified, while the 15.1 MeV γ-rays of the 1_2^+ state are not fully absorbed.

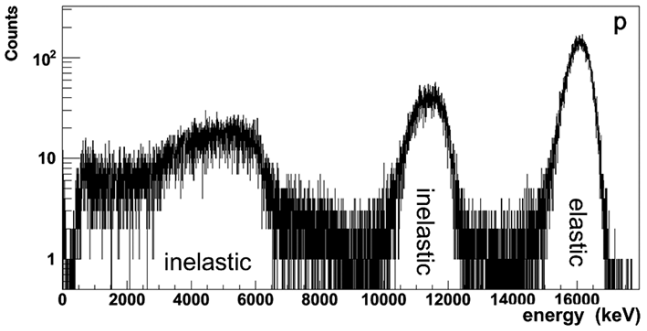

Fig. 8. Proton spectrum: The elastically scattered protons at 16 MeV and the inelastically scattered at 11.6 MeV that excite the 2_1^+ state can be identified. Additionally there is a broad distribution of protons that excite higher states in ^{12}C.

other way round it is feasible to determine the entire energy of a known particle that has only deposited part of its energy. The intersection of the partially stopped particles $N_{\mathrm{s,p,frac}}(N_\mathrm{f})$ with the function of the fully stopped particles $N_{\mathrm{s,p}}(N_\mathrm{f})$ provides this value. Applying this to the experimental results in fig. 5 means that, for instance, all events on the green line are elastically scattered protons whereas the blue line represents the inelastically scattered ones. The inelastically scattered protons with even less energy are stopped in the very beginning of the crystal and so the amount of protons that leave the crystal is strongly reduced. So a 2D function in N_s and N_f allows to reconstruct all intersection points and thus the particles incident energies numerically.

An energy spectrum of all events identified by RPID as γ-rays from the proton-carbon reaction is shown in fig. 7. At 4.4 MeV the first 2^+ state of ^{12}C, that decays via γ-radiation together with its single and double escape peak, can be identified. In principle there should also be the γ-peak for the 1_2^+ state at 15.1 MeV, but as simulations show positrons and electrons, that are mainly generated via pair production in the first interaction, emit bremsstrahlung photons with high energies escaping from the small detector setup and do not allow for a full energy absorption.

The energy spectrum of the fully stopped protons is shown in fig. 8.

The energy resolution here is dominated by the target thickness and by variation in energy loss due to not fully homogeneous wrapping layers. The peak at 16 MeV represents the elastically scattered protons whereas the inelastically scattered protons that excite the 2_1^+ state in ^{12}C can be identified with an energy of about 11.6 MeV. In the lower energy range there is a broad smearing of protons that are related to the population of higher-lying states, but due to the energy resolution they cannot be resolved.

5 Conclusion

In this paper we presented a new digital particle identification algorithm for CsI(Tl) scintillators based on a moving window deconvolution. By several processing steps (see fig. 1) the original preamplifier signal shape is simplified to allow for direct access on the two physical components in the scintillation light. Thereby all the used algorithms are designed to be implemented in an FPGA for real-time particle identification. Additionally we showed that it is possible to determine the energy of protons not fully absorbed within one crystal due to the non-linear N_s-to-N_f ratio in the energy range up to 16 MeV.

We thank R. Lang and M. Klöckner for the precise production of all mechanical parts of the detection system and would like to acknowledge the tandem operators who ensured a stable proton beam. We also want to thank S. Winkler for providing her clean room and mounting the detector devices, O. Tengblad for the fruitful discussions and R. Schneider for the assistance in modifying the preamplifiers. This work is supported by BMBF 06MT7178/06MT9156/06MT04NUP EraNet NupNet project GANAS, DFG Cluster of Excellence 153 "Origin and Structure of the Universe" and Maier-Leibnitz-Laboratorium, Garching.

References

1. R.S. Storey, W. Jack, A. Ward, Proc. Phys. Soc. **72**, 1 (1958) doi: 10.1088/0370-1328/72/1/302.
2. John D. Valentine, William W. Moses, Stephen E. Derenzo, David K. Wehe, Glenn F. Knoll, Nucl. Instrum. Methods Phys. Res. A **325**, 147 (1993) doi: 10.1016/0168-9002(93)91015-F.
3. R. Gwin, R.B. Murray, R.Murray, Phys. Rev. **131**, 501 (1963) doi: 10.1103/PhysRev.131.501.
4. P. Schotanus, R. Kamermans, IEEE Trans. Nucl. Sci. **37**, 177 (1990) doi: 10.1109/23.106614.
5. V. Nagirnyi, S. Zazubovich, V. Zepelin, M. Nikl, G.P. Pazzi, Chem. Phys. Lett. **227**, 533 (1994) doi: 10.1016/0009-2614(94)00857-4.
6. V. Nagirnyi, A. Stolovich, S. Zazubovich, V. Zepelin, E. Mihokova, E. Nikl, G.P. Pazzi, L. Salvini, J. Phys.: Condens. Matter **7**, 3637 (1995) doi: 10.1088/0953-8984/7/18/026.
7. Svetlana Zazubovich, Radiat. Meas. **33**, 699 (2001) doi: 10.1016/S1350-4487(01)00086-5.
8. V. Babin, K. Kalder, A. Krasnikov, S. Zazubovich, J. Lumin. **96**, 75 (2002) doi: 10.1016/S0022-2313(01)00215-0.

9. D. Horn, G.C. Ball, A. Galindo-Uribarri, E. Hagberg, R.B. Walker, R. Laforest, J. Pouliot, Nucl. Instrum. Methods Phys. Res. A **320**, 273 (1992) doi: 10.1016/0168-9002(92)90785-3.
10. E.V. Sysoeva, V.A. Tarasov, O.V. Zelenskaya, V.A. Sulyga, Nucl. Instrum. Methods Phys. Res. A **414**, 274 (1998) doi: 10.1016/S0168-9002(98)00011-4.
11. W. Skulski, M. Momayezi, Nucl. Instrum. Methods Phys. Res. A **458**, 759 (2001) doi: 10.1016/S0168-9002(00)00938-4.
12. D. Cortina, B. Jakobsson, *Technical Report for the Design, Construction and Commissioning of The CALIFA Barrel: The R3B CALorimeter for In Flight detection of gamma-rays and high energy charged pArticles* (2011).
13. T. Aumann, J. Jonson, *Technical Proposal for the design, construction, commissioning and operation of R3B, a universal setup for kinematical complete measurements of Reactions with Relativistic Radioactive Beams* (2005).
14. J. Alarja, A. Dauchy, A. Giorni, C. Morand, E. Pollaco, P. Stassi, R. Billerey, B. Chambon, B. Cheynis, D. Drain, C. Pastor, Nucl. Instrum. Methods Phys. Res. A **242**, 352 (1986) doi: 10.1016/0168-9002(86)90232-9
15. A. Georgiev, W. Gast, IEEE Trans. Nucl. Sci. **40**, 770 (1993) doi: 10.1109/23.256659.
16. A. Georgiev, W. Gast, R.M. Lieder, IEEE Trans. Nucl. Sci. **41**, 1116 (1994) doi: 10.1109/23.322868.
17. Steven W. Smith, *The scientist and engineer's guide to digital signal processing*, 1st edition (California Technical Publishing, San Diego and Calif, 1997).
18. J. Stein, F. Scheuer, W. Gast, A. Georgiev, Nucl. Instrum. Methods Phys. Res. B **113**, 141 (1996) doi: 10.1016/0168-583X(95)01417-9.
19. J.-P. Martin, C. Mercier, N. Starinski, C.J. Pearson, P.-A. Amaudruz, IEEE Trans. Nucl. Sci. **55**, 84 (2008) doi: 10.1109/TNS.2007.910853.
20. D.F. Measday, P.S. Fisher, A. Kalmykov, F.A. Nikolaev, A.B. Clegg, Nucl. Phys. **45**, 98 (1963) doi: 10.1016/0029-5582(63)90786-7.
21. F. Ajzenberg-Selove, Nucl. Phys. A **506**, 1 (1990) doi: 10.1016/0375-9474(90)90271-M.
22. T. Ikagawa, J. Kataoka, Y. Yatsu, T. Saito, Y. Kuramoto, N. Kawai, M. Kokubun, T. Kamae, Y. Ishikawa, N. Kawabata, Nucl. Instrum. Methods Phys. Res. A **538**, 640 (2005) doi: 10.1016/j.nima.2004.09.021.
23. J. Kataoka, T. Saito, Y. Kuramoto, T. Ikagawa, Y. Yatsu, J. Kotoku, M. Arimoto, N. Kawai, Y. Ishikawa, N. Kawabata, Nucl. Instrum. Methods Phys. Res. A **541**, 398 (2005) doi: 10.1016/j.nima.2005.01.081.
24. J. Kataoka, R. Sato, T. Ikagawa, J. Kotoku, Y. Kuramoto, Y. Tsubuku, T. Saito, Y. Yatsu, N. Kawai, Y. Ishikawa, N. Kawabata, Nucl. Instrum. Methods Phys. Res. A **564**, 300 (2006) doi: 10.1016/j.nima.2006.03.033.
25. T. Ikagawa, J. Kataoka, Y. Yatsu, N. Kawai, K. Mori, T. Kamae, H. Tajima, T. Mizuno, Y. Fukazawa, Y. Ishikawa, N. Kawabata, T. Inutsuka, Nucl. Instrum. Methods Phys. Res. A **515**, 671 (2003) doi: 10.1016/j.nima.2003.07.024.
26. Michael Bendel, *Entwicklung und Test einer digitalen Auslese für das CALIFA-Kalorimeter*, Master's thesis, Technische Universität München, München (2010).